Changes in surface albedo after fire in boreal forest ecosystems of interior Alaska assessed using MODIS satellite observations

Evan A. Lyons,[1] Yufang Jin,[2] and James T. Randerson[2]

Received 26 September 2007; revised 3 January 2008; accepted 4 February 2008; published 15 April 2008.

[1] We assessed the multidecadal effects of boreal forest fire on surface albedo using Moderate Resolution Imaging Spectroradiometer (MODIS) satellite observations within the perimeters of burn scars in interior Alaska. Fire caused albedo to increase during periods with and without snow cover. Albedo during early spring had a mean of 0.50 ± 0.03 for the first three decades after fire, substantially higher than that observed in evergreen conifer forests (0.34 ± 0.04). In older stands between 30 and 55 years, albedo showed a decreasing trend during early spring, probably from a growing spruce understory that masked surface snow and caused increases in both simple ratio (SR) and enhanced vegetation index (EVI). During summer, albedo decreased by 0.012 ± 0.005 in the year immediately after fire (from 0.112 ± 0.005 to 0.100 ± 0.010). In subsequent years, summer albedo increased rapidly at first and then more gradually, reaching a broad maximum in 20–35 year stands (0.135 ± 0.006). These measurements provide evidence for a well-developed deciduous shrub and tree phase during intermediate stages of succession. Averaged over the first 5 decades, shortwave surface forcing from fires was -6.2 W m^{-2} relative to an evergreen conifer control and -3.0 W m^{-2} relative to a control constructed from 2000 to 2003 preburn observations. These forcing estimates had a magnitude substantially smaller than previous estimates and suggest that, at a regional scale, evergreen conifer stand density may be lower than that inferred from chronosequence studies.

Citation: Lyons, E. A., Y. Jin, and J. T. Randerson (2008), Changes in surface albedo after fire in boreal forest ecosystems of interior Alaska assessed using MODIS satellite observations, *J. Geophys. Res.*, *113*, G02012, doi:10.1029/2007JG000606.

1. Introduction

[2] Over the last several centuries, the fire regime within interior Alaska has been controlled by a combination of human, climate, and ecosystem processes. *Lutz* [1955] provides qualitative evidence that Native Americans used fires extensively for a wide range of purposes during the 19th century, including insect control and hunting. With the discovery of gold in the Klondike in 1886, an influx of miners to the region caused even more burning, with many fires set to increase the availability of dry fuels for mining (and winter use) and to make prospecting easier [*Lutz*, 1955, 1959]. By the middle of the 20th century, attitudes toward fire had shifted considerably, with fire suppression a high priority among land managers to preserve timber resources [*Lutz*, 1953; *Pyne*, 1982]. From the 1940s to the 1970s, burned area in interior Alaska steadily declined with decadal means of 0.50, 0.43, 0.26, and 0.20 Mha/yr [*Barney*, 1971; *Foote*, 1983]. An improved fire control capability, including smoke jumpers that started work in 1959, has been credited for part of this downward trend [*Viereck*, 1973]. Low levels of burned area during the 1960s and 1970s also have been linked quantitatively with cooler and wetter conditions that were prevalent during this time [*Duffy et al.*, 2005; *Rupp et al.*, 2007]. More recently, burned area in North America has increased even though contributions from human-ignition have decreased [*Kasischke and Turetsky*, 2006], suggesting that with contemporary management strategies [*DeWilde and Chapin*, 2006], climate-linked controls on total burned area are becoming increasingly important.

[3] The large increases in northern surface air temperature expected over the next several centuries [*Christensen et al.*, 2007] will probably increase the frequency of burning in boreal forest ecosystems [*Flannigan et al.*, 2005], assuming that management approaches remain the same. Driving mechanisms include a lengthening of the fire season [*Westerling et al.*, 2006] and increasing mid-summer drought stress in conifer ecosystems [*Monson et al.*, 2005; *Welp et al.*, 2007]. Contemporary and future changes in burned area have important consequences for carbon fluxes [*Harden et al.*, 2000; *Kasischke et al.*, 2000; *Amiro et al.*, 2001; *Wirth et al.*, 2002] and feedbacks between boreal ecosystems and climate [*Kurz et al.*, 1995; *McGuire et al.*, 2006; *Randerson et al.*, 2006]. In this context, a central and unresolved issue is how species composition changes after fire and what the consequences are of these changes for biogeochemical cycling [*Van Cleve and Viereck*, 1981] and surface energy exchange [*Chambers and Chapin*, 2002].

[1]Department of Geography, University of California, Los Angeles, California, USA.
[2]Department of Earth System Science, University of California, Irvine, California, USA.

0148-0227/08/2007JG000606

[4] Postfire succession in boreal forests depends on several interactive controls including site drainage status, fire severity, seed availability, and fire interval effects [*Lutz*, 1955; *Viereck*, 1973; *Foote*, 1983; *Viereck et al.*, 1983; *Harper et al.*, 2002; *Johnstone and Kasischke*, 2005; *Johnstone and Chapin*, 2006]. In well-drained upland areas within interior Alaska, a typical white spruce (*Picea glauca*) successional sequence includes a tall shrub-sapling stage from 3 to 30 years, a well-defined deciduous broadleaf forest stage (aspen or paper birch) from ~30–130 years, and a final white spruce stage from 130 to over 300 years [*Van Cleve and Viereck*, 1981; *Dyrness et al.*, 1986]. In poorly drained areas, a typical black spruce (*Picea mariana*) sequence includes a tall shrub-sapling stage from 5 to 30 years followed immediately by a black spruce stage from 30 to 90 years [*Van Cleve and Viereck*, 1981; *Dyrness et al.*, 1986]. Aspen can establish during intermediate stages of a black spruce successional trajectory, perhaps as a result of a severe fire exposing mineral soil [*Viereck*, 1983], but most studies imply that establishment of a well-developed deciduous broadleaf forest is rare in poorly drained areas. At a regional scale, relatively little quantitative information exists about the importance of a deciduous broadleaf tree stage, and more generally, the frequency of occurrence of the different successional pathways that have been documented extensively in past work.

[5] The fire-induced changes in plant functional type described above influence surface energy exchange by several different pathways. Removal of the evergreen conifer canopy and establishment of grasses and deciduous shrubs and trees after fire causes surface broadband albedo to substantially increase during fall, winter, and spring as a result of increases in surface area of exposed snow [*Liu et al.*, 2005; *Amiro et al.*, 2006]. Summer albedo also increases above prefire levels because early successional plant functional types, including grasses and deciduous trees and shrubs, have leaves and branches with higher albedo than those of evergreen needleleaf trees [*Betts and Ball*, 1997; *Roberts et al.*, 2004; *Amiro et al.*, 2006; *McMillan and Goulden*, 2008]. Over an annual cycle, the dynamic range of albedo within boreal forest ecosystems is bounded by black carbon coatings (char) on vegetation and soil surfaces that have an albedo of 0.06 [*Chambers and Chapin*, 2002; *Chambers et al.* 2005] and snow that has an albedo between approximately 0.7 and 0.9 [*Greuell and Oerlemans*, 2005; *Stroeve et al.*, 2005].

[6] Sensible heat fluxes during summer decrease during early and intermediate stages of postfire succession. During the first decade after fire, sensible heat fluxes are low because removal of the canopy overstory reduces surface roughness [*Chambers et al.*, 2005]. This simultaneously increases surface soil temperatures, heat fluxes into the ground, and emission of longwave radiation into the atmosphere [*Liu et al.*, 2005]. In areas underlain by permafrost, postfire increases in ground heat fluxes cause a thickening of the active layer [*Viereck*, 1982], particularly in areas where much of the soil organic matter layer was consumed. Sensible heat fluxes may remain low during intermediate stages of succession because deciduous broadleaf trees have high canopy conductance and thus dissipate more available energy in the form of latent heat than conifers [*Baldocchi et al.*, 2000].

[7] As a consequence of the multidecadal effects of fire on albedo and sensible heat fluxes, it is likely that current and projected increases in fire activity [*Gillett et al.*, 2004; *Flannigan et al.*, 2005; *Kasischke and Turetsky*, 2006] will have a regional cooling effect. This is broadly supported by climate modeling studies that show northern air temperatures are reduced substantially when boreal forests are replaced by grasslands [*Bonan et al.*, 1992; *Thomas and Rowntree*, 1992]. Comparisons of biogeochemical versus biophysical effects of changing boreal forest cover suggest that global radiative forcing is close to zero in some parts of the boreal forest for the case of afforestation [*Betts*, 2000] and a changing fire regime [*Randerson et al.*, 2006]. Given that greenhouse gas effects on climate are globally distributed, but albedo-driven effects are regionally concentrated [*Ramaswamy et al.*, 2001], the radiative forcing studies described above along with other recent coupled carbon-climate model simulations [*Brovkin et al.*, 2004; *Bala et al.*, 2007] provide additional support for the idea that an increase in boreal forest fire activity may slow climate warming in northern regions. The net effect of fire on northern climate depends critically, however, on our understanding and representation of albedo, surface energy exchange, and cloud processes in climate models.

[8] Remote sensing observations have provided substantial insight about fire-induced changes in species composition and surface biophysics. In North America, normalized difference vegetation index (NDVI), fractional absorbed photosynthetically active radiation (fAPAR), and satellite-derived estimates of net primary production (NPP) recover to prefire levels after approximately 5–10 years [*Kasischke and French*, 1997; *Amiro et al.*, 2003; *Hicke et al.*, 2003; *Goetz et al.*, 2006]. Concurrently, year-to-year variability in NDVI increases during spring months [*Goetz et al.*, 2006] possibly as a result of increased snow exposure and variability [*Liu and Randerson*, 2008] and variability in the timing of leaf out in deciduous plant functional types. *McMillan and Goulden* [2008] show that surface brightness and albedo during summer also increases rapidly after fire, reaching a maximum after ~7–15 years and then declining exponentially to a minimum value in a 150 year black spruce stand. Trajectories of NDVI and surface albedo are likely to be regionally variable and depend on whether intermediate successional stages include a strong deciduous component [*Kasischke and French*, 1997].

[9] Here we combined Moderate Resolution Imaging Spectroradiometer (MODIS) observations of broadband and narrowband albedo [*Schaaf et al.*, 2002] with information from the Alaska Large Fire Database [*Kasischke et al.*, 2002] to systematically evaluate changes in surface albedo after fire within interior Alaska. Our goals were to quantify how fire-induced changes in surface albedo influence the shortwave surface radiation budget at a regional scale and to improve our understanding of how plant functional types vary during postfire succession. The former provides information about potential feedbacks between a changing disturbance regime and northern climate whereas the latter is important for understanding how a changing fire regime will impact ecosystem processes.

2. Data and Methods

[10] To assess postfire albedo changes, we combined satellite-derived broadband and spectral (narrowband) albedo

observations (for the 5 year period from 2000 to 2004) with burn perimeter data from the Alaskan Fire Service that covered the period from 1950 to 2004 [*Alaska State Geospatial Data Clearinghouse*, 2006].

2.1. BRDF and Albedo Data

[11] We used level 3 Bidirectional Reflectance Distribution Function (BRDF) data (collection 4) in seven spectral bands from the MODIS sensor aboard the Terra platform to derive actual total shortwave albedo. The global BRDF/albedo products (MOD43B1 and MOD43B3) have been operationally produced every 16 days from atmospherically corrected surface reflectance observations for each of 7 MODIS land bands at a 1 km resolution [*Schaaf et al.*, 2002]. The retrieval algorithm models surface reflectance at different illumination and viewing angles with a semi-empirical linear BRDF model [*Wanner et al.*, 1997]. The BRDF is integrated over the reflected radiation hemisphere to yield black-sky albedo for a specific illumination direction and is integrated further over the incident radiation hemisphere to yield white-sky albedo. All sky albedo is the best representation of actual surface albedo under realistic radiation and atmospheric conditions and can be approximated as a linear combination of black sky and white sky albedos weighted by the fractions of direct and diffuse solar radiation respectively [*Lewis and Barnsley*, 1994].

[12] Here we derived black sky albedo for the mean solar zenith angle during 3 hour intervals, since the MODIS black sky albedo is provided only at local solar noon [*Schaaf et al.*, 2002]. Daily mean all sky albedo was then derived by a combination of the 3 hourly black sky albedo and white sky albedo weighted by the 3 hourly monthly mean fraction of direct and diffuse solar radiation from the World Climate Research Programme/Global Energy and Water-Cycle Experiment (WCRP/GEWEX), surface radiation budget (SRB) data set [*Lewis and Barnsley*, 1994; *Stackhouse et al.*, 2000]. For the narrow-band (spectral) albedos that we report, we used white sky albedo only.

[13] The snow/ice backgrounds were flagged in the surface reflectance product [*Vermote et al.*, 2002]. The narrowband to broadband conversion uses linear combinations of all seven bands with different weighting coefficients for snow and snow-free pixels [*Liang et al.*, 2005; *Stroeve et al.*, 2005]. We used snow coefficients for all pixels from 3 December through 6 April (winter and early spring) and snow-free coefficients for all pixels from 25 May through 29 September (summer). For 7 April through 24 May and for 30 September through 2 December, coefficients were defined by the snow or snow-free condition of each pixel. Only the highest quality BRDF/albedo inversions were used in this analysis based on the quality assurance bits embedded in the MODIS BRDF/albedo product. We do not report December and January albedo observations because of limits on the availability of high quality data as a result of large solar zenith angles at high latitudes. For the annual mean shortwave surface forcing calculations we applied the mean of the first and last 16 day periods for which we did have high quality all sky albedo to December and January to obtain a full year of data.

2.2. Land Cover and Vegetation Indices

[14] The MODIS land cover product provides a global distribution of land cover types based on the International Geosphere-Biosphere Programme (IGBP) classification scheme [*Friedl et al.*, 2002]. The MODIS land cover algorithm uses two robust supervised classification methods, a univariate decision tree and an artificial neural network. The algorithm currently exploits both spectral and temporal information from MODIS observations. Main input data include one full year of the BRDF-adjusted nadir reflectance in 7 bands and enhanced vegetation index (EVI) data at a 16 day interval as well as metrics derived from phenological patterns. A database of land cover test sites, a geographic representation of global land cover types, was established for classification training and assessment [*Muchoney et al.*, 1999].

[15] Within our study region, the most abundant vegetation class was open shrubland (IGBP classification number 7). This class accounted for 25% of the interior area (40% of the unburned vegetation) and probably includes taiga ecosystems with relatively low density stands of black spruce. Evergreen needleleaf forest (IGBP classification number 1) accounted for 10.6% of the interior (17% of the unburned vegetation).

[16] To explore how albedo and canopy cover were linked, we extracted EVI from the 16 day MODIS Vegetation Indexes (MODIS VI) product (MOD13A2) [*Huete et al.*, 2002] within our study domain. EVI was specifically designed to limit soil background and atmospheric effects, thus enhancing the sensitivity of this index to changes in vegetation cover [*Gao et al.*, 2000]. We also derived simple ratio (SR) using the red and near infrared reflectance bands embedded in the MODIS VI product.

2.3. Fire Perimeter Observations

[17] The Alaskan Forest Service maintains a GIS database [*Alaska State Geospatial Data Clearinghouse*, 2006] that contains burn perimeter data for fires as far back as 1950 (Figure 1). Perimeters were mapped as polygons using a variety of methods including analysis of remote sensing data and helicopter and ground surveys [*French et al.*, 1995; *Kasischke et al.*, 2002]. The uncertainty of the actual fire location varies between ±200 m and ±500 m depending on when the perimeter was mapped and generally increases with the age of the fire [*Murphy et al.*, 2000]. Perimeter records are missing for 14%, 57%, 12%, 8%, and 0.2% of the total area burned for the 1950s, 1960s, 1970, 1980s, and 1990s, respectively [*Kasischke et al.*, 2002]. The large unmapped burned areas, particularly in the 1960s, were the result of records that were lost when they were combined to annual reports. The data set contains only fires greater than 1000 acres prior to and including 1988 and fires greater than 100 acres after 1988.

2.4. Solar Radiation

[18] We obtained monthly average 3 hourly incoming shortwave radiation data from NASA Langley Research Center [*Stackhouse et al.*, 2000]. It was derived with the shortwave algorithm of the GEWEX-SRB Project [*Pinker and Laszlo*, 1992]. The data covers the time period 1983–1995 and were generated on a nested grid, with a resolution of 1° latitude globally, and a longitudinal resolution ranging from 1° in the tropics and subtropics to 120° at the poles. The climatology of direct and diffuse solar radiation was used to derive the all sky surface albedo. The ratio of

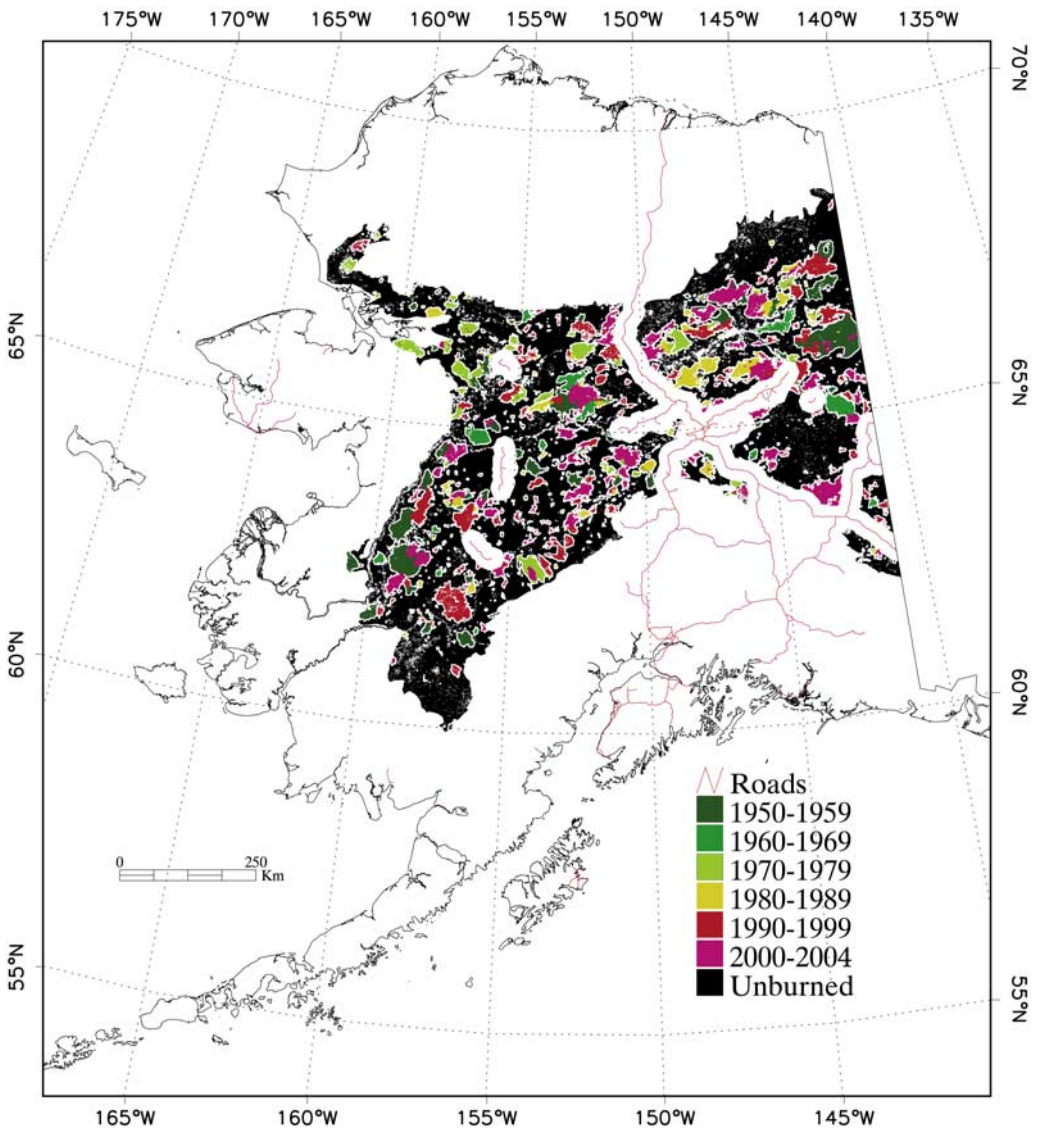

Figure 1. This map shows the boundaries of the study area, fire locations, buffer areas around fires, roads, and unburned areas. The Alaskan intermontane boreal interior is bounded by the Alaska Range to the south and the Brooks Range to the north. A 20 km buffer on either side of major roads was imposed to avoid vegetation transitions associated with agriculture or other forms of non-fire disturbance near human settlements. Fire perimeter data are from the Alaska Fire Service [*French et al.*, 1995; *Kasischke et al.*, 2002]. Ecoregion and road data are from the United States Geological Survey [*USGS*, 1999].

indirect to direct radiation varies from 100% indirect in December and January to 54% in May.

[19] For the shortwave surface forcing calculation, we used the 1961–1990 monthly mean observations of incoming shortwave radiation from the National Solar Radiation Data Base (NSRDB; http://rredc.nrel.gov/solar/old_data/nsrdb/1961–1990/). We constructed a mean time series from the six available sites in interior Alaska, including Bettles, Big Delta, Fairbanks, Gulkana, McGrath, and Talkeetna. This mean time series agreed reasonably well with measurements collected during 2002–2004 from towers near Delta Junction [*Randerson et al.*, 2006] (data not shown). We estimated reflected shortwave radiation at the surface by multiplying the monthly MODIS all sky albedo (described in section 2.1) by the NSRDB climatology of incoming shortwave radiation. We estimated the shortwave surface forcing as the difference between annual mean absorbed shortwave radiation for an individual age class of stands and a control. The two controls we defined and used are described in section 2.6.

2.5. Study Area and Analysis Approach

[20] We used a study area within the Alaskan interior that was identified by the Unified Ecoregions of Alaska: 2001 data set as "Intermontane Boreal" [*Nowacki et al.*, 2001] and had a total area of 466,140 km^2 (Figure 1 and Table 1). Only fires within this study area were analyzed. Fire perimeters accounted for approximately 5.8%, 2.1%, 2.8%, 2.9%, and 7.5% of the study area during the 1950s, 60s, 70s, 80s, and 90s, respectively. An additional 8.9%

Table 1. Distribution of Land Cover and Fires in Interior Alaska

Region	Area (km^2)	Percent of Interior (%)	Early Spring Albedo[a]	Summer Albedo[b]
Fires[c]	139991	30.0%	0.48 ± 0.05	0.129 ± 0.006
1950–1959	27077	5.8%	0.41 ± 0.06	0.125 ± 0.008
1960–1969	9800	2.1%	0.45 ± 0.05	0.134 ± 0.006
1970–1979	13090	2.8%	0.53 ± 0.06	0.142 ± 0.007
1980–1989	13542	2.9%	0.50 ± 0.06	0.130 ± 0.007
1990–1999	35121	7.5%	0.53 ± 0.04	0.129 ± 0.004
2000–2004[d]	41361	8.9%	0.44 ± 0.06	0.102 ± 0.008
Unburned[e]	306841	65.8%	0.43 ± 0.04	0.126 ± 0.006
Unburned evergreen conifer[f]	49638	10.6%	0.34 ± 0.04	0.112 ± 0.005
Unburned deciduous Broadleaf[f]	11210	2.4%	0.46 ± 0.06	0.134 ± 0.007
Unburned other[f,g]	245993	52.8%	0.45 ± 0.04	0.128 ± 0.006
Other	19308	4.1%	0.48 ± 0.04	0.116 ± 0.007
Water[f]	12226	2.6%	0.45 ± 0.04	0.108 ± 0.007
Wetlands, croplands, urban, snow/ice, barren[f]	7082	1.5%	0.55 ± 0.04	0.139 ± 0.007
Total interior area[h]	466140	100.0%	0.44 ± 0.04	0.126 ± 0.006

[a]The early spring period is defined as the four 16 day periods between 2 February and 6 April.
[b]The summer period is defined as the four 16 day periods between 10 June and 12 August.
[c]From the Alaska Large Fire Database (ALFD) [*Alaska State Geospatial Data Clearinghouse*, 2006].
[d]2000–2003 fires measured in 2000–2004, respectively.
[e]Unburned refers to areas outside of fire perimeters in the ALFD between 1950 and 2004 but within the intermontane boreal region. As such, it is likely that most of this area burned at some time prior to 1950. This area also includes post-1950 fires that were not recorded or for which fire perimeter data was not available.
[f]From the MODIS Land Cover Product, IGBP classification scheme [*Friedl et al.*, 2002].
[g]The four most abundant MODIS land cover classes in 'unburned other' are open shrublands, woody savannas, closed shrublands, and mixed forests, accounting for 25%, 12%, 8%, and 7% of the interior area, respectively.
[h]Defined as the 'Intermontane Boreal' by the Ecoregions of Alaska and Neighboring Territory 2001 Data set [*Nowacki et al.* 2001].

(41361 km^2) burned between 2000 and 2004 (Table 1). We imposed a two km (two pixel) buffer around burn perimeters, with one pixel inside and one pixel outside, to limit errors from inherent uncertainty in the burn perimeter vector data and from the process of conversion from vector to raster format. Areas within 20 km of major highways were excluded to limit possible land cover transitions associated with human activity. We also removed areas that were classified as water (IGBP classification number 0), permanent wetlands (11), croplands (12), urban and built up (13), cropland/natural vegetation mosaic (14), permanent snow and ice (15), and barren or sparsely vegetated (16), by the MODIS International Geosphere-Biosphere Programme (IGBP) Land Cover product [*Friedl et al.*, 2002]. These various filters remove 35.3% from the original interior leaving 301,537 pixels remaining. Table 2 summarizes the areas removed and retained for our analysis.

[21] To avoid errors introduced from small sample size, years with less than 10 pixels (after excluding buffer pixels and imposing the other constraints described above) or less than two fires were removed prior to our analysis (Table 3). These years included 1952, 1955, 1960–1967, and 1978.

2.6. Estimation of Prefire Albedo

[22] To compare different successional stages and as a standard for assessing the effect of fire on surface net shortwave radiation (shortwave surface forcing) it was necessary to estimate prefire albedo. We accomplished this using two different methods. We also defined a deciduous broadleaf forest end-member to enable comparisons with different postfire stand ages.

[23] The first estimate (hereafter referred to as the preburn control) was constructed by measuring the albedo before fires that occurred during the MODIS era; specifically fires that burned during 2001–2004 that we could sample prior to the fire event during 2000–2003. We averaged all pixels that had not yet burned for each 16 d period to build a seasonal climatology of prefire albedo. This control has the advantage of providing an estimate of prefire albedo exactly in the areas that burned, but requires the assumption that fires prior to 2000 were distributed across the landscape with the same vegetation and topographic distributions.

[24] As a second control (hereafter referred to as the MODIS conifer control), we used the set of all pixels classified by the MODIS Land Cover IGBP system as evergreen needleleaf forest (IGBP classification number 1) that were outside of fire perimeters from the Alaska Large Fire Database (described in section 2.3). An advantage of the MODIS conifer control is that it only includes pixels

Table 2. Retained and Excluded Areas in Albedo Analysis

Region	Area (km^2)	Percent of Region (%)
Removed		
Areas near human settlements[a]	71970	15.4%
Lakes and water	13622	2.9%
Barren, wetlands, croplands, urban, and snow/ice	8299	1.8%
Buffer areas	70712	15.2%
Total Removed	164603	35.3%
Retained		
Burned 1950–1959	18287	3.9%
Burned 1960–1969	5976	1.3%
Burned 1970–1979	8552	1.8%
Burned 1980–1989	7810	1.7%
Burned 1990–1999	18861	4.0%
Burned 2000–2004	21543	4.6%
Total burned	81029	17.4%
Unburned	220508	47.3%
Total retained	301537	64.7%
Total interior area	466140	100.0%

[a]We excluded areas within 20 pixels of either side of major roads to avoid agricultural areas and areas where human settlements may have impacted the disturbance regime via means other than fire.

Table 3. Fire Areas Used in Albedo Analysis for Each Year

Year	Number of Fires	Area (km^2)	Year	Number of Fires	Area (km^2)
1950	32	6832	1978	2	0*
1951	10	522	1979	21	1344
1952	1*	0*	1980	4	312
1953	5	294	1981	23	624
1954	16	2020	1982	3	55
1955	2	0*	1983	7	19
1956	10	984	1984	20	70
1957	57	6642	1985	19	496
1958	19	149	1986	52	673
1959	38	844	1987	21	85
1960	3	5*	1988	58	5407
1961	0*	0*	1989	12	69
1962	5	0*	1990	128	6691
1963	2	1*	1991	105	2720
1964	0	0*	1992	23	129
1965	1*	0*	1993	88	997
1966	1*	137	1994	75	306
1967	5	6*	1995	25	14
1968	20	403	1996	58	750
1969	28	5424	1997	91	5182
1970	7	19	1998	18	164
1971	31	990	1999	77	1908
1972	54	1468	2000	42	1704
1973	7	43	2001	17	230
1974	10	767	2002	79	5056
1975	4	106	2003	35	1186
1976	4	98	2004	123	13367
1977	36	3717			

*, Years with less than 10 pixels or less than 2 fires were excluded from the analysis.

dominated by evergreen needleleaf trees (probably mostly black spruce and white spruce in interior Alaska). This vegetation type covered 10.6% of interior Alaska (Table 1) and probably represents a reasonable baseline for surface shortwave forcing estimates in areas that have substantial tree cover. We defined, in parallel, a deciduous broadleaf forest end-member within the intermontane interior as the unburned area that was classified by the MODIS Land Cover IGBP system as deciduous broadleaf forest (IGBP classification number 4).

[25] Combined, these three sets of albedo provide benchmarks to assess postfire dynamics. The MODIS conifer control is probably a reasonable lower bound for prefire albedo derived from MODIS because it contains pixels dominated by dense evergreen needleleaf forests and excludes other areas such as open taiga, shrublands, and tundra that can also burn. Drawing conclusions solely from regions defined by MODIS land cover classes carries some risk because the classes themselves were defined in part by using MODIS reflectance phenologies [*Friedl et al.*, 2002]. The preburn control is defined independently and, as shown below, typically has higher albedo values than the MODIS conifer control.

3. Results

3.1. Postfire Changes in Albedo

[26] The Survey Line fire burned approximately 45,000 ha from 26 June through August 2001 near the Tanana River south and west of Fairbanks and provides an example of how broadband surface albedo typically changed during the first few years after a fire (Figure 2a). During and immediately after the fire, albedo decreased from 0.108 ± 0.001 during the 10–25 June period before the fire to a minimum of 0.070 ± 0.014 during 30 September to 15 October. With the onset of snow accumulation in the fall, albedo substantially increased above prefire levels (from ~0.3 during the fall of 2000 to ~0.5 during the fall of 2001). In subsequent years, during periods with snow cover, albedo remained elevated relative to prefire levels by about the same amount as during the first year. Summer albedo, in contrast, showed an increasing year-by-year trend. By 2004, mid-summer (10 June–12 August) albedo was 0.131 ± 0.005, and exceeded prefire albedo of 0.114 ± 0.006 observed during the same period in 2000. Analysis of all fires that occurred during 2000–2004 revealed a similar pattern to that observed for the Survey Line fire, including rapid recovery of summer albedo during the first several years and sustained increases in albedo during periods with snow cover (Figure 2b).

[27] Time series of broadband albedo from 2000 to 2004 for all retained fire perimeters from the 1950s, 1960s, 1970s, 1980s, and 1990s, along with the MODIS conifer control, are shown in Figure 3a. A mean seasonal cycle of

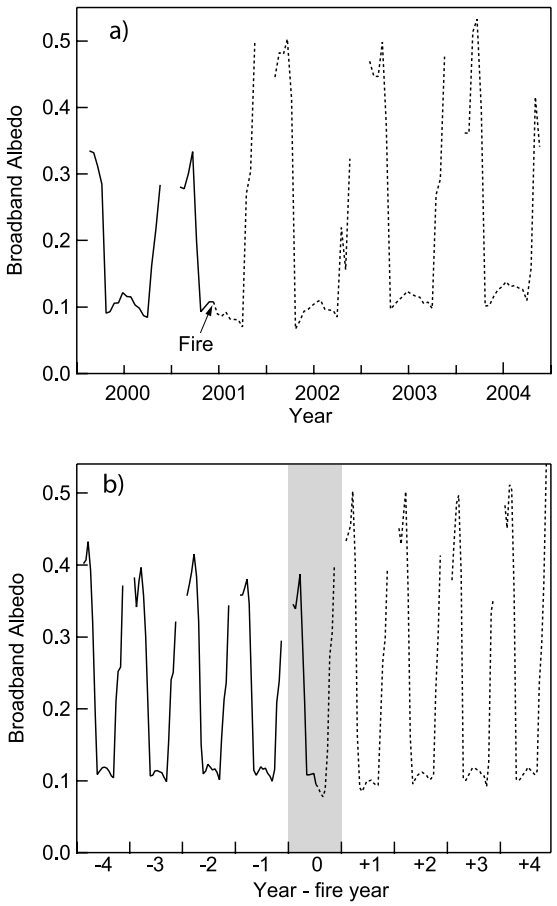

Figure 2. (a) Broadband albedo within the perimeter of the Survey Line fire that burned in interior Alaska during the summer of 2001. (b) Mean broadband albedo before and after all fires that occurred during the 2000–2004 period of satellite observations. The MODIS albedo data shown in both panels include all quality bits.

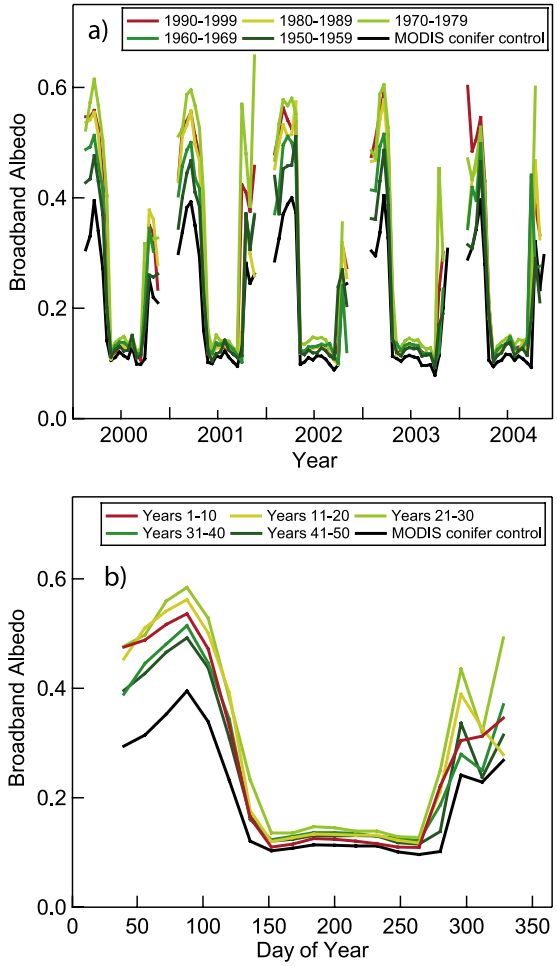

Figure 3. (a) Time series of broadband albedo during 2000–2004 averaged within burn perimeters from the 1950s to the 1990s. The MODIS conifer control is also shown in black. (b) Observations from all MODIS years were combined to form a mean seasonal cycle and averaged together for different sets of postfire stand ages. Stands between 21 to 30 years had the highest albedo during early spring and summer. The large decreases in albedo during spring in Figure 3b show that, on average across the intermontane boreal interior of Alaska, snowmelt started around day 100 (10 April) and was complete by day 150 (30 May).

albedo constructed from this time series is shown in Figure 3b, as a function of time since fire (or postfire stand age). Snow cover and vegetation phenology strongly modulated the annual cycle of albedo. During both early spring and summer, stands with ages between 21 and 30 years had the highest albedo, whereas the MODIS conifer control had the lowest.

[28] To examine how succession influences surface albedo, we sampled MODIS albedo from 2000 to 2004 within burn perimeters from 1950 to 2003. Postfire trajectories of albedo were constructed for early spring (Figure 4) and summer (Figure 5) periods, before and after the transitional snowmelt period that occurred primarily between 10 April (Julian day 100) and 30 May (Julian day 150) in the intermontane boreal interior (e.g., Figure 3b).

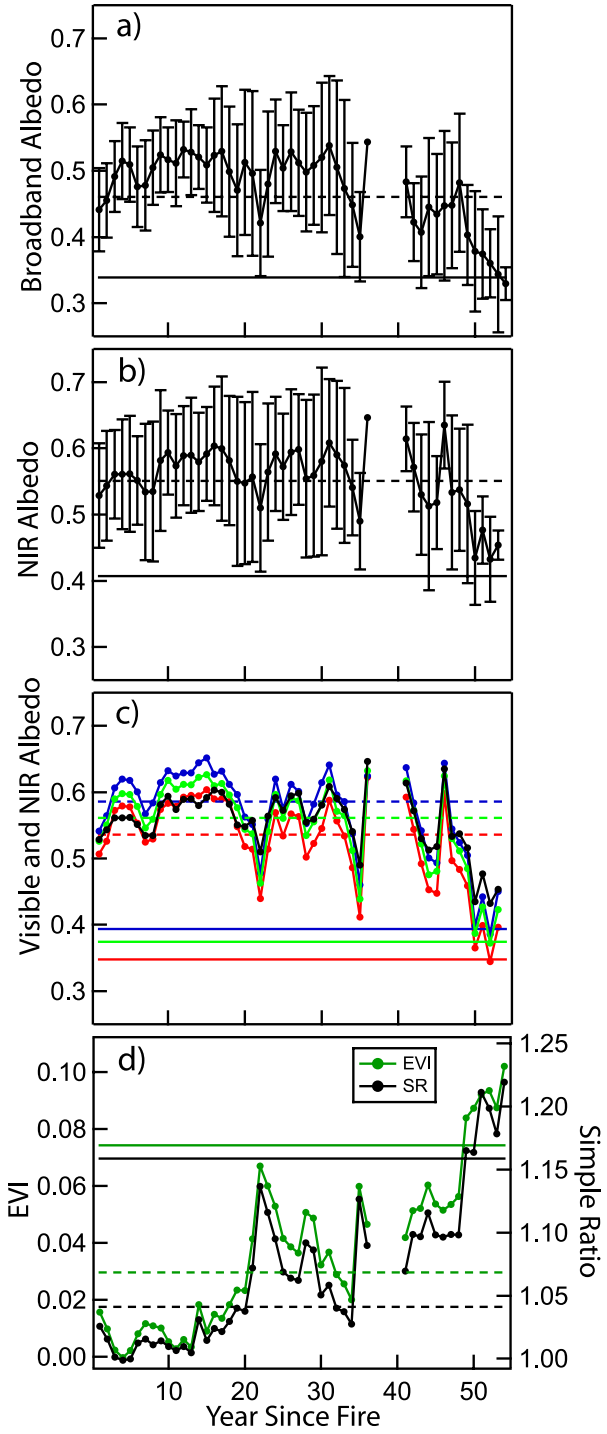

Figure 4. Broadband albedo, narrowband albedo, EVI, and SR are shown as functions of postfire stand age for a period before snowmelt during early spring (2 February–6 April). Horizontal lines represent the mean of the MODIS conifer control (solid) and the MODIS deciduous broadleaf forest end-member (dashed). (a) Broadband shortwave albedo with standard deviation error bars. (b) White sky NIR albedo with standard deviation error bars. (c) Blue, green, and red white sky albedo with NIR albedo added in black for comparison. (d) EVI and SR vegetation indices. EVI was obtained directly from the MOD13A2 vegetation indices product. SR was derived separately from the red and NIR surface reflectance bands provided as a part of this product.

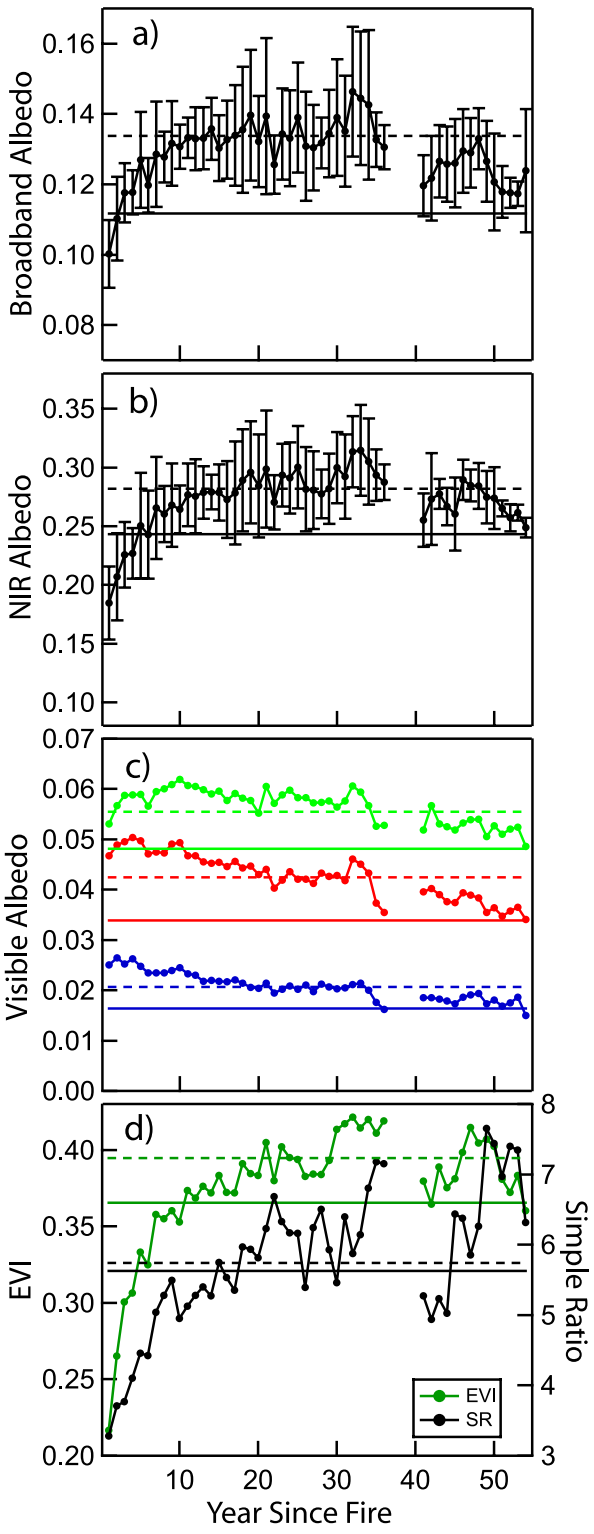

Figure 5. Same as Figure 4 but for summer (10 June–12 August).

[29] During early spring (2 February to 6 April), broadband albedo had a mean of 0.50 ± 0.03 for the first three decades after fire (Figure 4a). This level was substantially higher than the MODIS conifer control (0.34 ± 0.04) and slightly higher than the MODIS deciduous broadleaf forest end-member (0.46 ± 0.06). In stands older than 30 years, broadband albedo decreased and was approximately equal to the MODIS conifer control after 55 years.

[30] Near-infrared albedo (NIR albedo; 0.841–0.876 μm) for early spring remained relatively constant for the first 46 years after fire with a mean of 0.57 ± 0.03 (Figure 4b). This level was comparable to the MODIS deciduous broadleaf forest end-member (0.55 ± 0.05). NIR albedo decreased in stands older than 46 years but by an amount that was proportionally less than that observed for broadband albedo.

[31] A comparison of NIR and visible albedo provides evidence for an increasing role of plant canopies (and thus a decreasing role of snow) in shaping early spring albedo as a function of time since fire (Figure 4c). During the first 15 years, narrowband albedo was highest in the blue (0.459–0.479 μm) and lowest in the NIR. This pattern, with albedo decreasing across the visible and NIR parts of the spectrum, is consistent with the spectra obtained from snow [*Painter et al.*, 2003]. In contrast, for stands with ages between 45 and 54 years, NIR albedo was the highest and red albedo (0.620–0.670 μm) was the lowest. Although this shift is small and is probably not statistically robust, it suggests the emergence of the red edge (a large and sharp increase in reflectance between the red and NIR at ~0.7 μm) associated with the presence of chlorophyll [*Tucker*, 1979]. This trend is supported by the postfire trajectories of EVI and (SR) metrics derived separately from MODIS surface reflectance data (Figure 4d).

[32] During summer, broadband albedo was lower than the MODIS conifer control during the first year after fire, with a mean of 0.100 ± 0.010 as compared with 0.112 ± 0.005 for the conifer control (Figure 5a). In subsequent years, albedo increased, rapidly at first and then more slowly, reaching a mean of 0.135 ± 0.006 in stands 20–35 years after fire. These intermediate aged stands had a mean albedo that was equal to or exceeded the MODIS deciduous broadleaf forest end-member (which had a mean of 0.134 ± 0.007). Between 36 and 54 years after fire, albedo showed a decreasing (and variable) trend. Tower-based broadband albedo measurements within the perimeter of the Donnelly Flats fire [*Liu and Randerson*, 2008] show a reasonably good agreement with the MODIS estimates and provide additional support for rapid increases in albedo during the first few years after fire (Figure 6).

[33] The postfire trajectory of broadband albedo during summer (Figure 5a) had contrasting NIR (Figure 5b) and visible (Figure 5c) components. NIR albedo decreased substantially in the first year after fire to a minimum of 0.184 ± 0.031, and then quickly recovered reaching a maximum of 0.315 ± 0.039 at 33 years after fire. The magnitude of the NIR albedo change was substantially larger than that observed for broadband albedo. NIR albedo appeared to be primarily responsible for the initial decrease and recovery in broadband albedo during the first 35 years after fire because visible albedo was either mostly constant (green) or decreasing (red and blue) during this time (Figure 5c). Toward the end of the time series (between 36 and 54 years), in contrast, decreases in NIR and visible albedo contributed in parallel to the observed decreases in broadband albedo.

[34] EVI and SR during summer increased rapidly during the first decade after fire and then more slowly over the

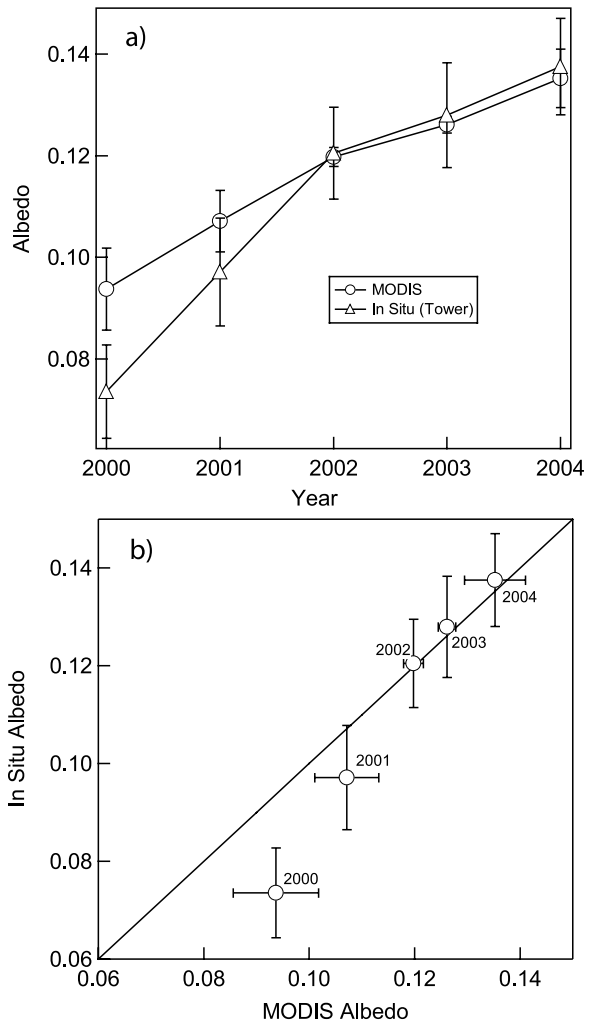

Figure 6. In situ measurements of broadband albedo during summer (10 June – 12 August) from a tower within the perimeter of the Donnelly Flats fire [*Liu and Randerson*, 2008] as compared with MODIS data extracted from within the burn perimeter, after removing a one pixel buffer. The Donnelly Flats fire occurred during June of 1999. The MODIS albedo data shown here includes all quality bits.

following two decades (Figure 5d). These indices remained high between 36 and 54 years even though NIR and broadband albedo decreased. This was probably caused by relatively large decreases in red reflectance during this period that offset the impacts of declining NIR reflectance.

3.2. Albedo and Elevation

[35] Within the intermontane boreal interior, burned area, fire return times, and the effect of fire on surface albedo varied with surface elevation (reported below with units of meters above sea level [m.a.s.l.]). Most of the burned area during 1950–2006 occurred within an elevation class of 0–200 m (with a total burned area of 6.1×10^4 km^2; Figure 7a), whereas the highest percentage of area burned occurred between 200 and 400m (Figure 7b). Fire return times varied between 160, 147, 180, 221, and 620 years for elevation classes of 0–200, 200–400, 400–600, 600–800, and greater than 800 m, respectively. These estimates are similar to an earlier analysis by *Kasischke et al.* [2002] and are probably biased high because of missing fire perimeter records in the Alaska Large Fire Database (see section 2.3).

[36] Early spring albedo for MODIS conifer control increased with both increasing and decreasing elevation from a minimum of 0.29 for the 400–600 m elevation class (Figure 7c). This pattern may be linked with sparser tree cover and increased snowfall at lower elevations toward the

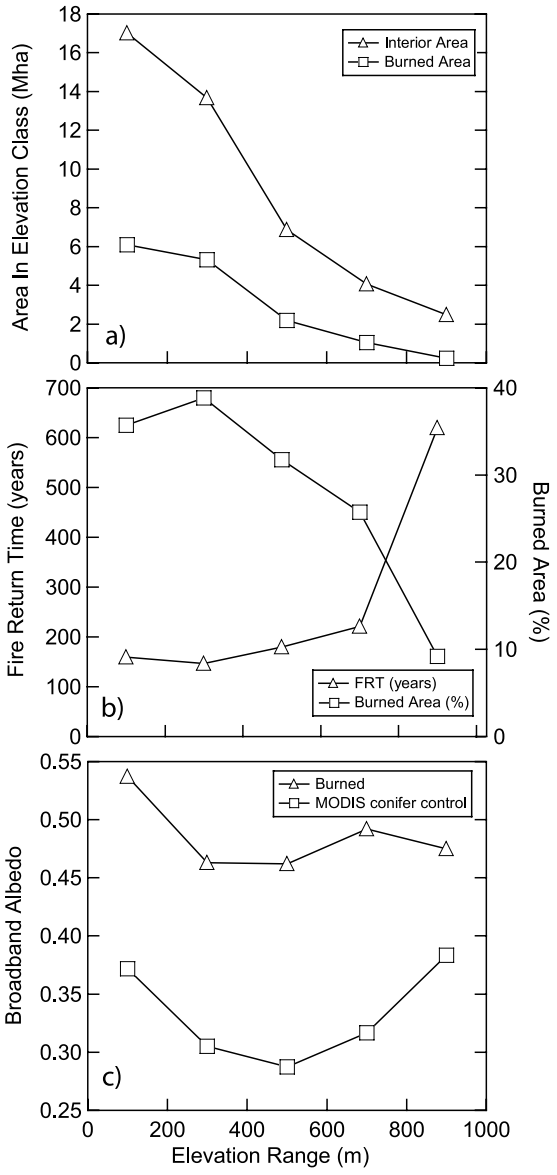

Figure 7. (a) Burned area and total area as a function of elevation within the intermontane boreal interior region of Alaska during 1950–2006. Over 96% of the interior area is below 1000 m. One million hectares (1 Mha) is equal to 10^{10} m^2. (b) Mean fire return time (left axis, triangles) and percent of area burned (right axis; open squares) for each elevation class during this 56 year period. (c) Early spring albedo (2 February to 6 April) for the MODIS evergreen control (open squares) and for the mean of stands with ages of 1–10 years after fire (open triangles).

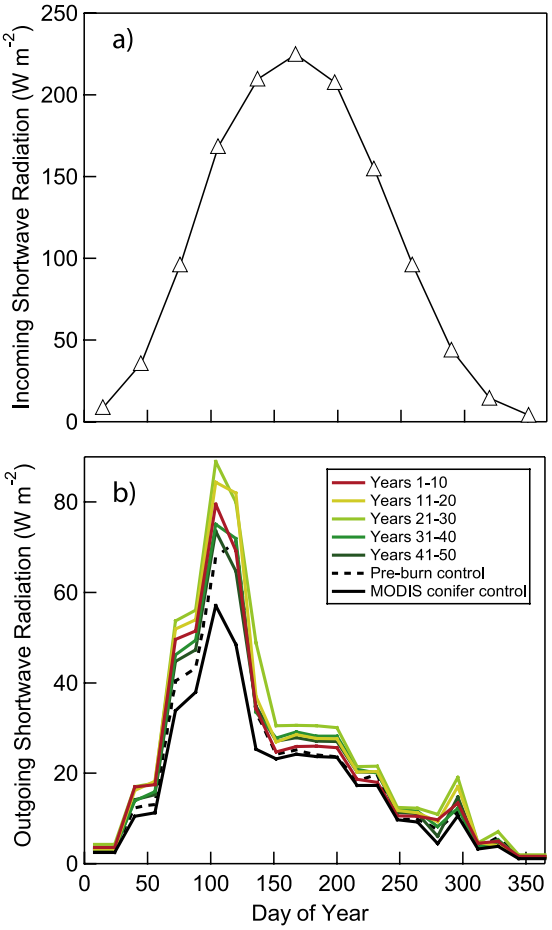

Figure 8. (a) Monthly mean incoming shortwave solar radiation at the surface in interior Alaska from the National Solar Radiation Data Base 1961–1990 mean. (b) Outgoing shortwave radiation at the surface. This flux was obtained by multiplying broadband all-sky albedo (Figure 3b) with incoming shortwave solar radiation shown in Figure 8a. The preburn control is shown with a dashed black line and the MODIS conifer control is shown with a solid black line.

west (toward the mouth of the Yukon River) and with increasing elevation in interior areas such as the Kuskokwim Mountains and the Tanana Uplands. During the first decade after fire, early spring albedo increased substantially, with a mean increase of 0.15 relative to the conifer control (Figure 7c). Unburned and postfire albedo differences were greatest at intermediate elevations (0.18 for 400–600 m and 600–800 m elevation classes). These differences were smaller below 400 m (0.16) and above 800 m (0.09).

3.3. Shortwave Surface Forcing From Fire-Induced Changes in Surface Albedo

[37] Monthly mean incoming shortwave solar radiation at the surface for the Alaskan interior varied substantially by season, from 4 W m^{-2} in December to 225 W m^{-2} in June (Figure 8a). We estimated outgoing shortwave radiation at the surface as the product of incoming radiation and all sky broadband albedo (Figure 8b). The seasonal maximum for outgoing shortwave radiation occurred between 7 April and 8 May for all age classes. This peak during spring occurred as a result of rapidly increasing incoming solar radiation (because of increasing day length) coupled with high albedo from the remaining snow cover. The largest value of 89 W m^{-2} occurred during the 7 April to 22 April period in 21–30 yr stands. These stands also have the highest outgoing flux when averaged over the full year (Figure 8b).

[38] We estimated shortwave surface forcing as the difference between absorbed shortwave radiation for an individual age class and a control. We used the same climatology of incoming solar radiation (Figure 8a) for all burn perimeters within the state, so that the differences across different stand age classes were due solely to changes in broadband albedo. The maximum surface forcing occurred between 7 April and 8 May for all age classes as shown by the outgoing radiation difference (Figure 8b). When calculated using the MODIS conifer control, mean annual shortwave surface forcing was −5.2, −7.0, −8.9, −5.3, and −4.5 W m^{-2} for stand age classes of 1–10, 11–20, 21–30, 31–40, and 41–50 years after fire, respectively (Figure 9). When calculated using the preburn control, surface forcing was −2.0, −3.8, −5.7, −2.1, and −1.3 W m^{-2} for the same set of stand age classes. Stands with ages of 21–30 years

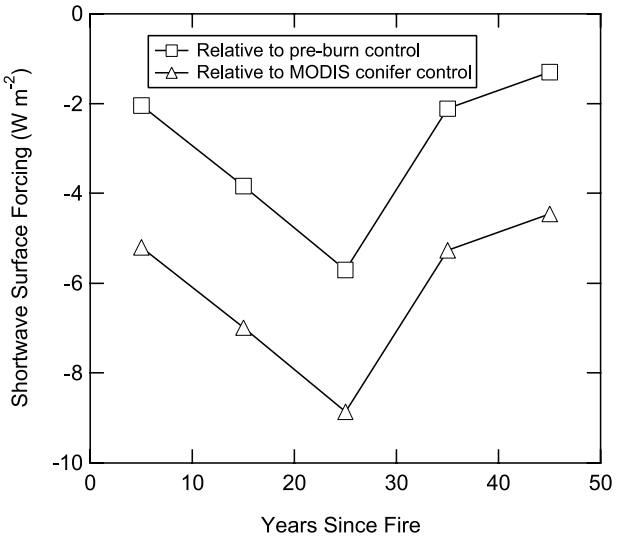

Figure 9. Shortwave surface forcing from fire effects on surface albedo was calculated relative to the preburn control (upper line) and the MODIS conifer control (lower line). These estimates represent an annual mean, taking into account variability across each 16 day period (e.g., Figure 8) and diurnal and seasonal variability in solar zenith angle effects on all sky surface albedo (as described in sections 2.1 and 2.4).To convert these shortwave surface forcing estimates to radiative forcing (at the tropopause following the IPCC convention), the effects of clouds and aerosols on outgoing shortwave radiation must be considered (see the supporting online material of *Randerson et al.* [2006]). For interior Alaska, *Randerson et al.* [2006] estimate that radiative forcing from albedo changes was approximately 60% of surface forcing based on calculations from a column radiation model that was calibrated using solar radiation observations from interior Alaska.

after fire had the most negative values of surface forcing as a result of high albedos during both summer and early spring.

4. Discussion

4.1. Implications for Postfire Succession

[39] During the first year after fire, summer broadband albedo and NIR albedo decreased substantially below prefire levels. Because narrowband visible albedo remained relatively constant or even increased, this implies large-scale replacement of living vegetation with black carbon on soil surfaces and on dead spruce boles. Summer broadband and NIR albedo increased rapidly in subsequent years probably as a result of several factors, including establishment and growth of early successional grass, forb, and shrub species, degradation and loss of the black carbon coating on soil surfaces and dead spruce boles, and initial growth of early successional moss species on the soil surface (including *Polytrichum spp.*). The MODIS trajectory of summer broadband albedo (Figure 5a) qualitatively agrees with measurements from *Chambers and Chapin* [2002] that show an initial reduction of albedo from 0.088 to 0.06 immediately after fire, followed by a rapid increase to 0.135 after 7 years.

[40] During intermediate stages of succession, MODIS observations provide evidence for a well-developed deciduous shrub and tree phase in many of the burn scars across the interior of Alaska. Stands between 20 and 35 years have a high broadband albedo during summer that is equal to or exceeds the MODIS deciduous broadleaf forest end-member (Figure 5). These stands also have spectral albedo and EVI measurements during summer and early spring that are similar to those from the deciduous end-member (Figures 4 and 5). While it is not possible to distinguish specifically between tall shrub and deciduous tree plant functional types, the dynamic range and continuity of the measurements suggest this may be possible in the future with additional field observations. Specifically, it may be possible to use measurements of canopy cover, stand density, and height for intermediate-aged stands that have a range of tree and shrub canopy cover to develop training data sets for classification approaches that take advantage of both the spectral and phenological variations in albedo shown in Figures 3–5.

[41] Between 30 and 55 years, increasing EVI during early spring (Figure 4d) is consistent with a growing spruce understory that masks snow and causes broadband albedo to decrease (Figure 4a). A growing spruce understory during this phase is also supported by decreasing albedo during summer in all bands (Figure 5). Although variable, high EVI and NIR albedo during summer in 45–50 year stands suggest deciduous trees may persist in the canopy overstory and as a result, summer albedo may more slowly converge on the conifer end-member than albedo during early spring. A synthesis of tower-based chronosequence measurements also shows diverging summer and winter trajectories of albedo after fire, and a more rapid recovery of albedo during winter to prefire levels [*Amiro et al.*, 2006]. It is likely that deciduous trees persist in the overstory after 55 years (the time limit of our current study), but gradually decrease in density as they are replaced by conifers. Evidence for this comes from a time series of Landsat measurements in Manitoba that show a decreasing trend in brightness and summer albedo for a 1930 burn that was sampled 54 to 75 years after fire [*McMillan and Goulden*, 2008].

[42] Early spring albedo also may provide insight about burn severity, a critical variable regulating fire emissions and post fire succession [*Johnstone and Kasischke*, 2005] that has been diagnosed in the past using summer Landsat observations [*Michalek et al.*, 2000; *Epting and Verbyla*, 2005; *Duffy et al.*, 2007]. Stands with a higher severity might be expected to have greater snow exposure after fire because of more complete consumption of the canopy overstory, fewer unburned islands, and deeper burning into the soil organic layer that would allow for the dead boles to fall over at a faster rate. In this respect, a metric based on the difference between pre and postfire broadband albedo during early spring (e.g., Figure 2) has potential to complement other remote sensing based approaches that have focused on summer observations, such as the normalized burn ratio derived from Landsat bands 4 and 7. With a longer time series from MODIS, it may be possible to link burn severity with different postfire trajectories of surface albedo, building on the approach described here. It is likely that even more information could be extracted from MODIS and Landsat remote sensing observations if the Alaska Large Fire Database were extended to earlier periods, even if this were for a subset of fire perimeters. A key question in this context is whether black spruce increases or decreases in density (and canopy cover) between 50 and 100 years and consequences for surface albedo and radiative forcing.

4.2. Shortwave Surface Forcing

[43] The annual mean shortwave surface forcing estimated here from MODIS over the first 5 decades after fire was -3.0 W m^{-2} based on the preburn control and -6.2 W m^{-2} based on the MODIS conifer control. These surface forcing estimates were 27% and 55% of that estimated for an individual fire based on tower-mounted pyranometer measurements (-11.2 W m^{-2} from the Supporting Online Material of *Randerson et al.* [2006]). It is likely that a combination of scaling and remote sensing-based factors contribute to this difference.

[44] First, the estimates presented here (Figure 9) are a mean over the entire intermontane boreal interior, an area of 46.6 Mha. Within this region, not all fires occur in closed-canopy evergreen needleleaf forest stands where the effects of fire on surface albedo are likely to be largest. For example, *Viereck* [1973] estimated that 43% of fires in the interior of Alaska occurred in tundra and only 36% in conifer forests. Similarly, the MODIS IGBP land cover algorithm classified 25.3% of the intermontane boreal interior as open shrubland (class 7) and only 10.6% as evergreen needleleaf forest (class 1). Fire-induced changes in surface albedo and forcing are likely to be considerably smaller in tundra and open taiga areas because, in the absence of an evergreen needleleaf canopy overstory, winter albedo is not likely to change substantially after fire. Further, high surface albedo in tundra ecosystems prior to fire during summer [*Chambers et al.*, 2005] may limit the magnitude of postfire increases that are typically observed in black spruce ecosystems [e.g., *Liu and Randerson*, 2008].

Fens, bogs, and other unburned islands within burn perimeters also probably reduce the magnitude of surface forcing.

[45] Another scaling related issue has to do with the density of boreal forest stands. The MODIS mean for snow covered albedo in unburned evergreen needleleaf forests was 0.34 ± 0.04, much higher than tower-based measurements from Canadian jack pine (0.15 ± 0.05) and black spruce (0.11 ± 0.09) [*Betts and Ball*, 1997] and the mean of mature conifer forests across Canada and Alaska (0.21) [*Amiro et al.*, 2006]. Some of the difference between MODIS and the tower observations may be explained if, on average, evergreen needleleaf forest stands have a lower tree density and more gaps than the sites that are typically chosen to represent these forests in tower-based chronosequence studies. A lower density of black spruce may also explain why MODIS summer albedo for the evergreen conifer class (0.112 ± 0.005; Table 1) is higher than ~0.08–0.09 mean that is typically reported in field studies [*Chambers and Chapin*, 2002; *Amiro et al.*, 2006; *McMillan and Goulden*, 2008].

[46] Many of these scaling issues also probably affect field-based estimates of fire emissions. For example, if forests on average have lower tree densities and more gaps, then aboveground fuel loads and postfire carbon accumulation rates may be lower than that inferred from chronosequence studies that draw upon measurements from higher density forests. Thus, any comparison of biogeochemical and biophysical climate forcing agents associated with a changing fire regime (e.g., greenhouse gas emissions versus surface albedo changes) requires consideration of how scaling issues simultaneously influence all of the agents.

[47] A final scale related issue has to do with uncertainties associated with the Alaska Large Fire Database. As described in section 2.3, the fire perimeter information for a number of fires from the 1950s and 1960s was lost and as a consequence these fires are not represented within the fire perimeter database. If some of these unmapped fires are included in either the evergreen conifer or preburn control areas, it would probably have the effect of reducing the magnitude of our estimates of shortwave surface forcing.

[48] A second class of reasons for the smaller forcing obtained here at a regional scale has to do with uncertainties in the satellite-derived estimates of surface albedo, especially during periods with snow cover. No single satellite-derived estimate of surface albedo functions perfectly under all conditions and it is likely that high accuracy can only be obtained at a regional scale by combining multiple satellite products with high quality surface and aircraft observations. There is some empirical evidence, for example, that MODIS estimates of pure snow albedo are low by ~2–7% [*Greuell and Oerlemans*, 2005; *Stroeve et al.*, 2005; *Salomon et al.*, 2006]. This type of bias would reduce the magnitude of the fire-induced changes in surface albedo during winter and spring (and consequently our estimates of shortwave surface forcing). Comparison of mid-day albedo from a tower within the perimeter of the Donnelly Flats fire [*Randerson et al.*, 2006] with MODIS observations during early spring supports this (0.61 ± 0.13 vs 0.41 ± 0.13), but is limited by a large mismatch in spatial scale.

[49] Another issue with consequences that are challenging to quantify arises from the MODIS BRDF/albedo retrieval algorithm in densely forested areas with varying snow cover. To avoid spurious results caused by variable or intermittent snow cover during a 16 day interval (i.e., during snowmelt) the MODIS algorithm defines each 16 day interval as either snow covered or snow-free based on the snow status of the majority of overpasses [*Schaaf et al.*, 2002]. In retrieving the BRDF, non-snow overpasses are excluded if the majority of individual overpasses are designated as snow covered (and vice-versa). For snow covered pixels in areas with forest cover, snow-free overpasses may be removed from the BRDF inversion if they are classified as snow-free as a consequence of snow settling underneath the evergreen forest canopy. This would have the effect of causing a high bias in MODIS-retrieved surface albedo in densely forested areas (and would reduce estimates of shortwave surface forcing during early spring when this pixel is compared with postfire pixels that have a high albedo). The utilization of snow coefficients for narrowband to broadband conversion may also contribute to about 5–10% high bias in total shortwave albedo over dense conifer forests. Another uncertainty comes from the atmospheric correction under snow conditions. A constant aerosol optical depth of 0.05 was applied to derive surface reflectance over snow [*Vermote et al.*, 2002]. This under-corrected aerosol effect may contribute to a high bias for dark surfaces and a low bias for bright surfaces [*Li and Garand*, 1994], which also reduces the magnitude of albedo change and thus the shortwave surface forcing estimates.

[50] Resolving both the scaling issues and the uncertainties associated with the satellite retrievals described above requires additional information and provides motivation for an aircraft campaign in interior Alaska or another northern region to measure components of the radiation budget. Flight transects across a range of forest stand ages (e.g., Figure 1) and topography during snow covered and snow-free periods would provide critical validation for albedo estimates derived from MODIS, MISR, and Landsat satellite observations. Given the large mismatch in spatial scale between the footprint of tower-mounted radiometers and the pixel size of satellite observations, aircraft measurements appear essential for advancing our understanding of the processes that regulate the albedo of snow covered forests at a regional scale.

4.3. Implications of a Changing Fire Regime

[51] Aspects of the fire cycle in boreal forests that may be sensitive to climate change include the frequency of burning in different ecosystem types, the size and number of large fire events, burn severity, and the seasonal cycle of burned area and emissions [*Kasischke et al.*, 2002]. The elevation distribution of fires may also respond to a changing climate. Soil temperatures and permafrost development, which are controllers of succession, depend on elevation, aspect, and drainage [*Viereck et al.*, 1986]. Poorly drained, north facing upland sites often are dominated by black spruce while dry, south facing sites contain white spruce or deciduous stands. Elevations above the alpine tree line burn infrequently. Decreases in albedo after fire are smaller for burns at higher elevations (Figure 7) probably because stands are not as dense before fire.

[52] Movement of fires into higher elevations with climate change may allow spruce forests to advance upwards in elevation over the long-term. Lower albedo from an

increased abundance of spruce may offset the cooling effect caused by increased fire activity and albedo at lower elevations within the interior. This change in land cover would have consequences for the surface energy balance and for feedbacks with climate [*Chambers and Chapin*, 2002].

[53] The timescales of different forcing agents associated with a changing fire regime are also challenging to quantify. For example, surface albedo dynamics after fire persist for at least 4–5 decades (Figures 4 and 5) and probably even longer. As a result, more frequent fires would increase the abundance of young stands and raise albedo at a regional scale. Concurrently, greenhouse gas concentrations would increase, contributing to warming. Ocean and terrestrial uptake would absorb some of the CO_2 emitted by an increase in fire activity, but some would remain in the atmosphere for centuries. In contrast, black carbon deposition on the Greenland ice sheet could lead to more solar radiation absorption [*Flanner et al.*, 2007], with possible consequences for centennial to millennial dynamics of this ice sheet.

5. Conclusions

[54] We assessed the long-term effects of boreal forest fire on surface albedo using MODIS satellite observations within the perimeter of burn scars in interior Alaska. Our measurements provided evidence for a strong deciduous phase in 20–35 year stands. Evidence for a developing spruce canopy between 35 and 55 years after fire was based on decreasing trends in NIR and visible narrowband albedo during early spring and summer and increases in EVI and SR during early spring. More generally, the high quality MODIS data show that it is possible to track the legacy of fire for boreal forest ecosystem structure and composition for at least 4–5 decades with a moderate (1 km) spatial resolution.

[55] After fire, annual outgoing shortwave radiation increased and was at a maximum in 21–30 yr stands. This had a cooling effect on climate although when quantified using the concept of shortwave surface forcing, our MODIS-based estimates had a smaller magnitude than previous estimates based on tower-mounted pyranometers [*Randerson et al.*, 2006]. This difference may be attributed to a combination of scaling and remote sensing issues. At a regional scale, estimates of surface forcing may be smaller if (1) evergreen conifer stand density is lower than what is typically measured in tower-based chronosequence studies, (2) if fires sometimes burn into more open taiga and tundra ecosystems, and (3) if unburned islands remain within burn perimeters. A clear step forward in terms of resolving these issues and remaining uncertainties associated with the remote sensing observations would be aircraft campaigns during spring and summer that are closely coordinated with ground and satellite observations systems. More generally, this study emphasizes the importance of the biogeophysical climate impacts associated with changes in high latitude forest cover that must be taken into account when calculating the costs and benefits of boreal forest management.

[56] **Acknowledgments.** We thank M. Mu, F. M. Kai, and P. Ling for comments on earlier drafts. This work was supported by a NASA grant to J. Randerson (NNG04GK49G).

References

Alaska State Geospatial Data Clearinghouse (2006), Alaska Fire Service geographic information system database of fire perimeters (akfirehist05.shp), Accessed June 2006. (Available at http://agdc.usgs.gov/data/blm/fire/)

Amiro, B. D., J. B. Todd, B. M. Wotton, K. A. Logan, M. D. Flannigan, B. J. Stocks, J. A. Mason, D. L. Martell, and K. G. Hirsch (2001), Direct carbon emissions from Canadian forest fires, 1959–1999, *Can. J. For. Res.*, *31*, 512–525, doi:10.1139/cjfr-31-3-512.

Amiro, B. D., J. I. MacPherson, R. L. Desjardins, J. M. Chen, and J. Liu (2003), Postfire carbon dioxide fluxes in the western Canadian boreal forest: evidence from towers, aircraft and remote sensing, *Agric. For. Meteorol.*, *115*, 91–107, doi:10.1016/S0168-1923(02)00170-3.

Amiro, B. D., et al. (2006), The effect of postfire stand age on the boreal forest energy balance, *Agric. For. Meteorol.*, *140*, 41–50, doi:10.1016/j.agrformet.2006.02.014.

Bala, G., K. Caldeira, M. Wickett, T. J. Phillips, D. B. Lobell, C. Delire, and A. Mirin (2007), Combined climate and carbon-cycle effects of large-scale deforestation, *Proc. Natl. Acad. Sci. U.S.A.*, *104*, 6550–6555, doi:10.1073/pnas.0608998104.

Baldocchi, D., F. M. Kelliher, T. A. Black, and P. Jarvis (2000), Climate and vegetation controls on boreal zone energy exchange, *Glob. Change Biol.*, *6*, 69–83, doi:10.1046/j.1365-2486.2000.06014.x.

Barney, R. J. (1971), Selected 1966–1969 interior Alaska wildfire statistics with long-term comparisonss, 13 pp., Pac. Northwest For. and Range Experiment Stn., U.S. For. Serv., Fairbanks, Alaska.

Betts, R. A. (2000), Offset of the potential carbon sink from boreal forestation by decreases in surface albedo, *Nature*, *408*, 187–190, doi:10.1038/35041545.

Betts, A. K., and J. H. Ball (1997), Albedo over the boreal forest, *J. Geophys. Res.*, *102*, 28,901–28,910, doi:10.1029/96JD03876.

Bonan, G. B., D. Pollard, and S. L. Thompson (1992), Effects of boreal forest vegetation on global climate, *Nature*, *359*, 716–718, doi:10.1038/359716a0.

Brovkin, V., S. Sitch, W. von Bloh, M. Claussen, E. Bauer, and W. Cramer (2004), Role of land cover changes for atmospheric CO2 increase and climate change during the last 150 years, *Glob. Change Biol.*, *10*, 1253–1266, doi:10.1111/j.1365-2486.2004.00812.x.

Chambers, S. D., and F. S. Chapin (2002), Fire effects on surface-atmosphere energy exchange in Alaskan black spruce ecosystems: Implications for feedbacks to regional climate, *J. Geophys. Res.*, *107*, 8145, doi:10.1029/2001JD000530[printed *108*(D1), 2003].

Chambers, S. D., J. Beringer, J. T. Randerson, and F. S. Chapin (2005), Fire effects on net radiation and energy partitioning: Contrasting responses of tundra and boreal forest ecosystems, *J. Geophys. Res.*, *110*, D09106, doi:10.1029/2004JD005299.

Christensen, J. H., et al. (2007), Regional climate projections, in *Climate Change 2007: The Physical Science Basis. Contribution of Working Group I to the Fourth Assessment Report of the Intergovernmental Panel on Climate Change*, edited by S. Solomon et al., pp. 847–940, Cambridge Univ. Press, New York.

DeWilde, L., and F. S. Chapin (2006), Human impacts on the fire regime of interior Alaska: Interactions among fuels, ignition sources, and fire suppression, *Ecosystems (N. Y., Print)*, *9*, 1342–1353, doi:10.1007/s10021-006-0095-0.

Duffy, P. A., J. E. Walsh, J. M. Graham, D. H. Mann, and T. S. Rupp (2005), Impacts of large-scale atmospheric-ocean variability on Alaskan fire season severity, *Ecol. Appl.*, *15*, 1317–1330, doi:10.1890/04-0739.

Duffy, P. A., J. Epting, J. M. Graham, T. S. Rupp, and A. D. McGuire (2007), Analysis of Alaskan burn severity patterns using remotely sensed data, *Int. J. Wildland Fire*, *16*, 277–284, doi:10.1071/WF06034.

Dyrness, C. T., L. A. Viereck, and K. Van Cleve (1986), Fire in taiga communities of interior Alaska, in *Forest Ecosystems in the Alaskan Taiga, Ecol. Ser.*, vol. 57, edited by K. Van Cleve et al., pp. 74–86, Springer, New York.

Epting, J., and D. Verbyla (2005), Landscape-level interactions of prefire vegetation, burn severity, and postfire vegetation over a 16-year period in interior Alaska, *Can. J. For. Res.*, *35*, 1367–1377, doi:10.1139/x05-060.

Flanner, M. G., C. S. Zender, J. T. Randerson, and P. J. Rasch (2007), Present-day climate forcing and response from black carbon in snow, *J. Geophys. Res.*, *112*, D11202, doi:10.1029/2006JD008003.

Flannigan, M. D., K. A. Logan, B. D. Amiro, W. R. Skinner, and B. J. Stocks (2005), Future area burned in Canada, *Clim. Change*, *72*, 1–16, doi:10.1007/s10584-005-5935-y.

Foote, M. J. (1983), Classification, description, and dynamics of plant communities after fire in the taiga of interior Alaska, Res. Pap. *PNW-307*, p. 116, U.S. Dep. of Agric., Portland, Oreg.

French, N. H. F., E. S. Kasischke, L. L. Bourgeau-Chavez, and D. Berry (1995), Mapping the location of wildfires in Alaskan boreal forests using AVHRR imagery, *Int. J. Wildland Fire*, *5*, 55–62, doi:10.1071/WF9950055.

Friedl, M. A., et al. (2002), Global land cover mapping from MODIS: algorithms and early results, *Remote Sens. Environ.*, *83*, 287–302, doi:10.1016/S0034-4257(02)00078-0.

Gao, X., A. R. Huete, W. G. Ni, and T. Miura (2000), Optical-biophysical relationships of vegetation spectra without background contamination, *Remote Sens. Environ.*, *74*, 609–620, doi:10.1016/S0034-4257(00)00150-4.

Gillett, N. P., A. J. Weaver, F. W. Zwiers, and M. D. Flannigan (2004), Detecting the effect of climate change on Canadian forest fires, *Geophys. Res. Lett.*, *31*, L18211, doi:10.1029/2004GL020876.

Goetz, S. J., G. J. Fiske, and A. G. Bunn (2006), Using satellite time-series data sets to analyze fire disturbance and forest recovery across Canada, *Remote Sens. Environ.*, *101*, 352–365, doi:10.1016/j.rse.2006.01.011.

Greuell, W., and J. Oerlemans (2005), Validation of AVHRR- and MODIS-derived albedos of snow and ice surfaces by means of helicopter measurements, *J. Glaciol.*, *51*, 37–48, doi:10.3189/172756505781829575.

Harden, J. W., S. E. Trumbore, B. J. Stocks, A. Hirsch, S. T. Gower, K. P. O'Neill, and E. S. Kasischke (2000), The role of fire in the boreal carbon budget, *Glob. Change Biol.*, *6*, 174–184, doi:10.1046/j.1365-2486.2000.06019.x.

Harper, K. A., Y. Bergeron, S. Gauthier, and P. Drapeau (2002), Postfire development of canopy structure and composition in black spruce forests of Abitibi, Quebec: A landscape scale study, *Silva Fennica*, *36*, 249–263.

Hicke, J. A., G. P. Asner, E. S. Kasischke, N. H. F. French, J. T. Randerson, G. J. Collatz, B. J. Stocks, C. J. Tucker, S. O. Los, and C. B. Field (2003), Postfire response of North American boreal forest net primary productivity analyzed with satellite observations, *Glob. Change Biol.*, *9*, 1145–1157, doi:10.1046/j.1365-2486.2003.00658.x.

Huete, A., K. Didan, T. Miura, E. P. Rodriguez, X. Gao, and L. G. Ferreira (2002), Overview of the radiometric and biophysical performance of the MODIS vegetation indices, *Remote Sens. Environ.*, *83*, 195–213, doi:10.1016/S0034-4257(02)00096-2.

Johnstone, J. F., and F. S. Chapin (2006), Fire interval effects on successional trajectory in boreal forests of northwest Canada, *Ecosystems (N. Y., Print)*, *9*, 268–277, doi:10.1007/s10021-005-0061-2.

Johnstone, J. F., and E. S. Kasischke (2005), Stand-level effects of soil burn severity on postfire regeneration in a recently burned black spruce forest, *Can. J. For. Res.*, *35*, 2151–2163, doi:10.1139/x05-087.

Kasischke, E. S., and N. H. F. French (1997), Constraints on using AVHRR composite index imagery to study patterns of vegetation cover in boreal forests, *Int. J. Remote Sens.*, *18*, 2403–2426, doi:10.1080/014311697217684.

Kasischke, E. S., and M. R. Turetsky (2006), Recent changes in the fire regime across the North American boreal region - Spatial and temporal patterns of burning across Canada and Alaska, *Geophys. Res. Lett.*, *33*, L09703, doi:10.1029/2006GL025677.

Kasischke, E. S., N. H. F. French, K. P. O'Neill, D. D. Richter, L. L. Bourgeau-Chavez, and P. A. Harrell (2000), Influence of fire on long-term patterns of forest succession in Alaskan boreal forests, in *Fire, Climate Change, and Carbon Cycling in the Boreal Forest*, edited by E. S. Kasischke and B. J. Stocks, pp. 214–235, Springer, New York.

Kasischke, E. S., D. Williams, and D. Barry (2002), Analysis of the patterns of large fires in the boreal forest region of Alaska, *Int. J. Wildland Fire*, *11*, 131–144, doi:10.1071/WF02023.

Kurz, W. A., M. J. Apps, B. J. Stocks, and W. J. A. Volney (1995), Global climate change: Disturbance regimes and biospheric feedbacks of temperate and boreal forests, in *Biotic Feedbacks in the Global Climate System: Will the Warming Speed the Warming?*, edited by G. M. Woodwell and F. Mackenzie, pp. 119–133, Oxford Univ. Press, Oxford, UK.

Lewis, P., and M. Barnsley (1994), Influence of the sky radiance distribution on various formulations of the earth surface albedo, *Proc. Mesures Physiques et Signatures en Teledection*, 707–716.

Li, Z. Q., and L. Garand (1994), Estimation of surface albedo from space - A parameterization for global application, *J. Geophys. Res.*, *99*, 8335–8350, doi:10.1029/94JD00225.

Liang, X. Z., et al. (2005), Development of land surface albedo parameterization based on Moderate Resolution Imaging Spectroradiometer (MODIS) data, *J. Geophys. Res.*, *110*, D11107, doi:10.1029/2004JD005579.

Liu, H., and J. T. Randerson (2008), Interannual variability of surface energy exchange depends on stand age in a boreal forest fire chronosequence, *J. Geophys. Res.*, *113*, G01006, doi:10.1029/2007JG000483.

Liu, H., J. T. Randerson, J. Lindfors, and F. S. Chapin (2005), Changes in the surface energy budget after fire in boreal ecosystems of interior Alaska: An annual perspective, *J. Geophys. Res.*, *110*, D13101, doi:10.1029/2004JD005158.

Lutz, H. J. (1953), The effects of forest fires on the vegetation of interior Alaska, 36 pp., Alaska For. Res. Cent., U.S. Dep. of Agric., Juneau.

Lutz, H. J. (1955), Ecological effects of forest fires in the interior of Alaska, 121 pp., U. S. Dep. of Agric., Alaska For. Res. Cent., U.S. For. Serv., Juneau.

Lutz, H. J. (1959), Aboriginal man and white man as historical causes of fires in boreal forest, with particular reference to Alaska, 49 pp., Yale Univ. Sch. of For, New Haven.

McGuire, A. D., F. S. Chapin, J. E. Walsh, and C. Wirth (2006), Integrated regional changes in arctic climate feedbacks: Implications for the global climate system, *Annu. Rev. Environ. Resour.*, *31*, 61–91, doi:10.1146/annurev.energy.31.020105.100253.

McMillan, A. M. S., and M. L. Goulden (2008), Age-dependent variations in the biophysical properties of boreal forests, *Global Biogeochem. Cycles*, doi:10.1029/2007GB003038, in press.

Michalek, J. L., N. H. F. French, E. S. Kasischke, R. D. Johnson, and J. E. Colwell (2000), Using Landsat TM data to estimate carbon release from burned biomass in an Alaskan spruce forest complex, *Int. J. Remote Sens.*, *21*, 323–338, doi:10.1080/014311600210858.

Monson, R. K., J. P. Sparks, T. N. Rosenstiel, L. E. Scott-Denton, T. E. Huxman, P. C. Harley, A. A. Turnipseed, S. P. Burns, B. Backlund, and J. Hu (2005), Climatic influences on net ecosystem CO_2 exchange during the transition from wintertime carbon source to springtime carbon sink in a high-elevation, subalpine forest, *Oecologia*, *146*, 130–147, doi:10.1007/s00442-005-0169-2.

Muchoney, D., A. Strahler, J. Hodges, and J. LoCastro (1999), The IGBP DISCover confidence sites and the system for terrestrial ecosystem parameterization: Tools for validating global land-cover data, *Photogrammetric Engineering and Remote Sensing*, *65*, 1061–1067.

Murphy, P. J., J. P. Mudd, B. J. Stocks, E. S. Kasischke, D. Barry, M. E. Alexander, and N. H. F. French (2000), Historical fire records in the North American boreal forest, in *Fire, Climate Change and Carbon Cycling in the Boreal Forest*, edited by E. S. Kasischke and B. J. Stocks, pp. 274–288, Springer, New York.

Nowacki, G., P. Spencer, T. Brock, M. Fleming, and T. Jorgenson (2001), *Ecoregions of Alaska and neighboring terroitory*, U. S. Geol. Surv., Reston, Va.

Painter, T. H., J. Dozier, D. A. Roberts, R. E. Davis, and R. O. Green (2003), Retrieval of subpixel snow-covered area and grain size from imaging spectrometer data, *Remote Sens. Environ.*, *85*, 64–77, doi:10.1016/S0034-4257(02)00187-6.

Pinker, R. T., and I. Laszlo (1992), Modeling surface Sslar Iirradiance fot satellite applications on a global scale, *J. Appl. Meteorol.*, *31*, 194–211, doi:10.1175/1520-0450(1992)031<0194:MSSIFS>2.0.CO;2.

Pyne, S. J. (1982), *Fire in America: A Cultural History of Wildland and Rural Fire*, 654 pp., Princeton Univ. Press, Princeton, N. J.

Ramaswamy, V., O. Boucher, J. Haigh, D. A. Hauglustaine, J. Haywood, G. Myhre, T. Nakajima, G. Y. Shi, and S. Solomon (2001), Radiative forcing of climate change, in *Climate Change 2001: The Scientific Basis. Contributions of Working Group 1 to the Third Assessment Report of the Intergovernmental Panel on Climate Change*, edited by J. T. Houghton et al., pp. 350–416, Cambridge Univ. Press, New York.

Randerson, J. T., et al. (2006), The impact of boreal forest fire on climate warming, *Science*, *314*, 1130–1132, doi:10.1126/science.1132075.

Roberts, D. A., S. L. Ustin, S. Ogunjemiyo, J. Greenberg, S. Z. Dobrowski, J. Q. Chen, and T. M. Hinckley (2004), Spectral and structural measures of northwest forest vegetation at leaf to landscape scales, *Ecosystems (N. Y., Print)*, *7*, 545–562, doi:10.1007/s10021-004-0144-5.

Rupp, T. S., X. Chen, M. Olson, and A. D. McGuire (2007), Sensitivity of simulated boreal fire dynamics to uncertainties in climate drivers, *Earth Interact.*, *11*.

Salomon, J. G., C. B. Schaaf, A. H. Strahler, F. Gao, and Y. F. Jin (2006), Validation of the MODIS Bidirectional Reflectance Distribution Function and Albedo retrievals using combined observations from the Aqua and Terra platforms, *IEEE Trans. Geosci. Remote Sens.*, *44*, 1555–1565, doi:10.1109/TGRS.2006.871564.

Schaaf, C. B., et al. (2002), First operational BRDF, albedo nadir reflectance products from MODIS, *Remote Sens. Environ.*, *83*, 135–148, doi:10.1016/S0034-4257(02)00091-3.

Stackhouse, P. W. J., S. K. Gupta, S. J. Cox, M. Chiacckio, and J. C. Mikovitz (2000), The WCRP/GEWEX Surface Radiation Budget Project Release 2: An assessment of surface fluxes at 1 degree resolution, paper presented at International Radiation Symposium, St. Petersburg, Russia, 24–29 July.

Stroeve, J., J. E. Box, F. Gao, S. L. Liang, A. Nolin, and C. Schaaf (2005), Accuracy assessment of the MODIS 16-day albedo product for snow: comparisons with Greenland in situ measurements, *Remote Sens. Environ.*, *94*, 46–60, doi:10.1016/j.rse.2004.09.001.

Thomas, G., and P. R. Rowntree (1992), The boreal forests and climate, *Q. J. R. Meteorol. Soc.*, *118*, 469–497, doi:10.1002/qj.49711850505.

Tucker, C. J. (1979), Red and photographic infrared linear combinations for monitoring vegetation, *Remote Sens. Environ.*, *8*, 127–150, doi:10.1016/0034-4257(79)90013-0.

USGS (1999), Major roads of the United States, Reston, Va., Oct.

Van Cleve, K., and L. A. Viereck (1981), Forest succession in relation to

nutrient cycling in the boreal forest of Alaska, in *Forest Succession: Concepts and Application*, edited by D. C. West, H. H. Shugart, and D. B. Botkin, pp. 185–211, Springer, Berlin.

Vermote, E. F., N. Z. El Saleous, and C. O. Justice (2002), Atmospheric correction of MODIS data in the visible to middle infrared: first results, *Remote Sens. Environ.*, *83*, 97–111, doi:10.1016/S0034-4257(02)00089-5.

Viereck, L. A. (1973), Wildfire in the taiga of Alaska, *Quat. Res.*, *3*, 465–495, doi:10.1016/0033-5894(73)90009-4.

Viereck, L. A. (1982), Effects of fire and firelines on active layer thickness and soil temperatures in interior Alaska, paper presented at 4th Canadian Permafrost Conference, The Roger J. E. Brown Memorial Volume, Natl. Res. Counc. of Can., Ottawa, Ont., Canada.

Viereck, L. A. (1983), The effects of fire in black spruce ecosystems of Alaska and northern Canada, in *The Role of Fire in Northern Circumpolar Ecosystems*, edited by R. W. Wein and D. A. MacLean, pp. 201–220, John Wiley, Chichester.

Viereck, L. A., C. T. Dyrness, K. Vancleve, and M. J. Foote (1983), Vegetation, soils, and forest productivity in selected forest types in interior Alaska, *Can. J. For. Res.*, *13*, 703–720, doi:10.1139/x83-101.

Viereck, L. A., K. Van Cleve, and C. T. Dyrness (1986), Forest ecosystem distribution in the taiga environment, in *Forest Ecosystems in the Alaskan Taiga*, edited by K. Van Cleve et al., pp. 22–43, Springer, New York.

Wanner, W., A. H. Strahler, B. Hu, P. Lewis, J. P. Muller, X. Li, C. L. B. Schaaf, and M. J. Barnsley (1997), Global retrieval of bidirectional reflectance and albedo over land from EOS MODIS and MISR data: Theory and algorithm, *J. Geophys. Res.*, *102*, 17,143–17,161, doi:10.1029/96JD03295.

Welp, L. R., J. T. Randerson, and H. P. Liu (2007), The sensitivity of carbon fluxes to spring warming and summer drought depends on plant functional type in boreal forest ecosystems, *Agric. For. Meteorol.*, *47*, 172–185, doi:10.1016/j.agrformet.2007.07.010.

Westerling, A. L., H. G. Hidalgo, D. R. Cayan, and T. W. Swetnam (2006), Warming and earlier spring increase western US forest wildfire activity, *Science*, *313*, 940–943, doi:10.1126/science.1128834.

Wirth, C., C. I. Czimczik, and E. D. Schulze (2002), Beyond annual budgets: carbon flux at different temporal scales in fire-prone Siberian Scots pine forests, *Tellus, Ser. B*, *54*, 611–630.

Y. Jin and J. T. Randerson, Department of Earth System Science, University of California, Irvine, CA 92697, USA.

E. A. Lyons, Department of Geography, University of California, Los Angeles, CA 90095, USA. (elyons@ucla.edu)